Environmental Science and Pollution Research (2022) 29:6633–6645
https://doi.org/10.1007/s11356-021-16119-z

RESEARCH ARTICLE

Impacts of horseradish peroxidase immobilization onto functionalized superparamagnetic iron oxide nanoparticles as a biocatalyst for dye degradation

Basem E. Keshta[1] · Ali H. Gemeay[1] · Abeer A. Khamis[2]

Received: 5 March 2021 / Accepted: 19 August 2021 / Published online: 28 August 2021

Abstract

To enhance the dye removal efficiency by natural enzyme, horseradish peroxidase (HRP) was immobilized onto amine-functionalized superparamagnetic iron oxide and used as a biocatalyst for the oxidative degradation of acid black-HC dye. The anchored enzyme was characterized by vibrating sample magnetometry, Fourier transform infrared spectroscopy, X-ray diffraction, thermogravimetry, scanning electron microscopy, Brunauer–Emmett–Teller and Barrett–Joyner–Halenda methods, nitrogen adsorption–desorption measurements, Zeta potential, energy dispersive X-ray spectroscopy, and transmission electron microscopy. The Michaelis constant values of free and immobilized HRP were determined to be 4.5 and 5 mM for hydrogen peroxide and 12.5 and 10 mM for guaiacol, respectively. Moreover, the maximum values of free and immobilized HRP were 2.4 and 2 U for H_2O_2, respectively, and 1.25 U for guaiacol. The immobilized enzyme was thermally stable up to 60°C, whereas the free peroxidase was stable only up to 40°C. In the catalytic experiment, the immobilized HRP exhibited superior catalytic activity compared with that of free HRP for the oxidative decolorization and removal of acid black-HC dye. The influence of experimental parameters such as the catalyst dosage, pH, H_2O_2 concentration, and temperature on the removal efficiency was investigated. The reaction followed second-order kinetics, and the thermodynamic activation parameters were determined.

Keywords Horseradish peroxidase · Immobilization · Enzymatic kinetic · 3-aminopropyltrimethoxysilane

Introduction

Enzymes are biocatalysts that facilitate complex chemical reactions under benign experimental and environmental conditions (Min and Yoo 2014; Ding et al. 2015). Specifically, peroxidase enzymes, which are isolated from many plant sources such as horseradish, are cheaper than microbial production sources and exhibit a wide range of applications including those in diagnostic kits and immunoassays such as ELISA, catalysis, wastewater treatment, treatment of pollutants such as phenols, organic and polymer synthesis, biosensor technology, and alignment of paper and pulp. In addition, peroxidase enzymes play a critical role in several industrial applications in the analytical, agriculture, environmental, and medical fields and are also used to determine hydrogen peroxide in industrial and biological tests (Rudra et al. 2008; Pandey et al. 2017).

Soluble enzymes are normally unstable and difficult to reuse and to isolate from the substrate and the product (Bilal et al. 2017b). In addition, they are inhibited by substrates, products, and other components, which limit their stability (Garcia-Galan et al. 2011). Immobilization is often resorted to as a means of overcoming these issues because it improves enzyme stability, resistance to inhibitors, and enzyme selectivity or specificity by altering the conformation of the enzyme after immobilization (Mateo et al. 2007). This approach is particularly effective for enhancing the thermal stability of enzymes, broadening their pH working range, and improving the recovery of the product (Min and Yoo 2014; Hoffmann et al. 2018). Enzyme immobilization is also applied to solve problems associated with limited enzyme solubility (Katchalski-Katzir 1993), improve the control of the reaction

Responsible Editor: Santiago V. Luis

✉ Abeer A. Khamis
abeer.khamis@science.tanta.edu.eg

[1] Chemistry Department, Faculty of Science, Tanta University, Tanta 31527, Egypt

[2] Biochemistry Division, Chemistry Department, Faculty of Science, Tanta University, Tanta 31527, Egypt

while allowing the use of various reactor configurations, and prevent contamination of the product, which is particularly important in food chemistry (Katchalski-Katzir 1993). Overall, enzyme immobilization is a powerful tool for circumventing these disadvantages and providing better properties for practical applications. In addition, it helps in maintaining the enzyme activity upon reuse (Iyer and Ananthanarayan 2008). Immobilization improves the enzyme stability through multipoint covalent attachment, multisubunit immobilization of multimeric proteins, or generation of favorable enzyme environments (Bilal and Iqbal 2021). Different immobilization techniques have been reported, including physical adsorption (Ali et al. 2018; Vineh et al. 2018a), covalent bonding (Vineh et al. 2018b), entrapment, crosslinking, and encapsulation (Bilal et al. 2017a, b). The two most widely used strategies of immobilizing enzymes without support are cross-linked enzyme crystals (CLECs) or aggregates (CLEAs) (López-Serrano et al. 2002).

Adsorption, covalent bonding, ionic bonding, encapsulation, and other more advanced forms of immobilization can be used to join the supports and the enzyme (Cipolatti et al. 2016). The simplest technique is adsorption, which allows enzymes to be immobilized on solid substrates via low-energy connections such as van der Waals or hydrophobic interactions, hydrogen bonds, and ionic bonds (Cipolatti et al. 2016). One effective immobilization strategy is using pre-existing solids whether porous or non-porous materials. The kind and physical properties of the solid support are effects on enzyme performance. Especially non-porous materials are special cases that have many merits but have some disadvantages that affect enzyme loading such as non-flexible and handle in the reactor and increase from protein contamination that impairs the volumetric activity (Garcia-Galan et al. 2011).

Ion exchange immobilization of enzymes is a multistep process in which the enzyme is attached to the carrier when the differential charge interactions are strong enough to compensate for the medium's ionic strength (Tong et al. 2002; Lyddiatt 2002). The isoelectric point is the pH at which the global protein charge is equal to zero. When the operational pH is greater than the protein's isoelectric point, it will have a negative net charge and will interact with positively charged exchange media. When the operational pH is lower than the protein's isoelectric point, it retains a positive net charge and thus interacts with negative exchange agents (Williams and Frasca 2001). Furthermore, enzymatic immobilization via ionic/electrostatic interactions is an adsorption immobilization strategy known as the ion-exchange policy. It is simple, quick, and inexpensive. It consists of the addition of the enzyme and support under adsorption-friendly conditions, with strict pH and ionic strength control (Tomotani and Vitolo 2006; Garcia-Galan et al. 2011). Because the physical bond is typically weak, this technique does not alter the native enzyme structure and avoids disturbances to enzyme active sites, allowing for the retention of enzyme catalytic activity. In contrast, due to weak interactions, enzyme retention and stabilization become a problem, as small changes in the medium's pH or ionic strength can cause desorption and subsequent loss of enzymes.

The increase in the enzyme activity by immobilization on nanoparticles (NPs) is related to the enzyme configuration, orientation, and density on the NP surface (Zhang et al. 2011; Guzik et al. 2014). The morphology of the NPs also has a significant impact. Kumar et al. demonstrated that HRP covalently immobilized in epoxy functional polypropylene films afforded a 90% removal efficiency in the catalytic degradation of basic red dye with about 90% removal (Kumar et al. 2016). Bilal et al. covalently immobilized HRP on calcium alginate using glutaraldehyde as a crosslinker agent with 85% immobilization efficiency (Bilal et al. 2016). Moreover, immobilized HRP exhibited 99% of residual activity after 10 min and was used as a biocatalyst for degradation of dyes. Nanayakkara et al. immobilized HRP on silica nanorods and applied the resulting solid surface as an oxidative catalyst for the polymerization of substituted phenol (Nanayakkara et al. 2014). The supported enzyme exhibited substantial catalytic activity compared with the free enzyme. Moreover, three different-shaped mesoporous silica NPs were prepared and used to immobilize HRP, achieving considerable catalytic activity (Yang et al. 2018). The immobilization of HRP onto magnetic supports has emerged as an innovative strategy for the development of biocatalysts for wastewater treatment (Donadelli et al. 2018). Surface silanization of magnetite NPs is the most widely used approach for introducing surface functional groups (such as NH_2) because it provides low cytotoxicity, good stability, and ease of performance in organic and aqueous solvents (Hosseinifar et al. 2017; Ramalingam et al. 2018).

In the current study, the use of the immobilized HRP enzyme in the decolorization of AB dye is discussed. Some parameters were studied to improve the degradation efficiency by increasing its stability by using pre-existing non-porous solid support through the physical adsorption immobilization technique. Also, choosing Fe_3O_4@NH_2 as solid support will limit the drawbacks of nonporous materials in non-flexible and handle in the reactor depending on paramagnetic properties. Moreover, the biochemical characterization of the immobilized HRP was assessed and compared with the free HRP.

Materials and methods

Chemicals and reagents

Ferrous sulfate heptahydrate, anhydrous ferric chloride, sodium hydroxide, methyl alcohol, toluene, and 3-aminopropyltrimethoxysilane (APTES) were purchased from Alpha Aesar. Horseradish (Armoracia rusticana) roots were purchased locally. Hydrogen peroxide and guaiacol were purchased from Sigma Chemical. Acid black-HC (AB) dye was

provided by Misr Spinning & Weaving Company, El-Mahalla El-Kubra, Gharbia, Egypt under project cooperation with Tanta University with grant number TU-03-16.

Synthesis

Synthesis of amine-functionalized magnetite NPs (Fe_3O_4@NH_2)

Fe_3O_4@NH_2 was synthesized according to previously published methods (Pasternack et al. 2008; Liu et al. 2013). Briefly, 2.5 g of dried powder of Fe_3O_4 NPs, which was prepared following a reported procedure (Gemeay et al. 2019), was poured into a 500 mL mixed solvent of methanol and toluene with equal volumes. Subsequently, the solution mixture was dispersed for 30 min under sonication, followed by slow addition of 10 mL APTES. The reaction was kept under mechanical overhead stirring at 70°C for 6 h. The particles obtained were washed with water and finally with ethanol to produce a fine powder. The powder was then dried in an oven for 12 h at 80°C.

Immobilization protocol of HRP

The immobilization protocol must take several factors into account, including the support properties, the active group of the support used to immobilize the enzyme, and that of the enzyme molecule, as well as the immobilization protocol itself. Only a careful selection of these three factors allows one to fully benefit from the immobilization process (Boudrant et al. 2020). First, the Fe_3O_4@NH_2 NPs were washed repeatedly with double-distilled water. For the immobilization of HRP onto the surface of Fe_3O_4@NH_2, 5 mg enzyme (4500 units of enzyme) was dissolved in a 50 mL acetate buffer at pH 5.6 and mixed gently with Fe_3O_4@NH_2 at room temperature (RT) overnight. The Fe_3O_4@NH_2-HRP product was dried for one night at RT (Mohamed et al. 2008). In summary, HRP was immobilized onto Fe_3O_4@NH_2 (preexisting solid support) using the physical adsorption immobilization method (Garcia-Galan et al. 2011; Jesionowski et al. 2014).

Characterization methods

The functionalization and immobilization of HRP onto the magnetite surface were confirmed using Fourier transform infrared (FT-IR) spectroscopy using a JASCO FT-IR-4100 (Japan) spectrometer in the $\dot{\upsilon}$ range of 4000–200 cm^{-1} and thermogravimetric analysis (TGA) on a Shimadzu TG-50-TA (Japan) in a temperature range from 25 to 800°C with a flow rate of 5°C min^{-1} under N_2. The crystalline structure of the prepared samples was studied using X-ray diffraction (XRD) in a GNR, APD 2000 PRO diffractometer (Italy) operating at a beam current of 40 kV and 30 mA and 2θ = 2–80° at a scan rate of 0.05°/step. The JCPDS database was used to analyze the diffraction peaks observed. The surface measurements of catalysts were recorded on Brunauer–Emmett–Teller (BET) NONA touch 4LX (USA) and Barrett–Joyner–Halenda (BJH) NONA touch 4LX (USA). The dispersion of the catalyst in solution was confirmed using zeta potential analysis (Santa Barbara, CA, USA). The magnetic properties of the as-prepared samples were measured using a handmade vibrating sample magnetometer (VSM, Tanta, Egypt) (El-Alaily et al. 2015). An ultraviolet–visible (UV–vis) T80+ double-beam was used to monitor the AB dye concentration in the solution. The morphology of the catalyst surface, the particle size, and elemental analysis were studied using a transmission electron microscope (TEM, JEM-2100F (USA) and a scanning electron microscope (SEM, FEI Quanta environmental) integrated with an octane silicon drift detector (SDD) to deliver high-quality energy dispersive X-ray (EDX) data (EDAX, AMETEK).

Kinetics measurements

The decolorization process became remarkable after the addition of H_2O_2 and Fe_3O_4@NH_2-HRP to the AB solution at the same time. The decrease in the AB concentration was monitored using a UV–vis spectrophotometer at λ_{max} = 575 nm. Moreover, the absorption data were fitted to a second-order kinetic plot, according to Eq. (1). The oxidation of AB was performed in a 250-mL Erlenmeyer flask in a shaker thermostat with a speed of 150 rpm. In detail, 300 mg of Fe_3O_4@NH_2-HRP, 2.4×10^{-4} M of AB, and 0.16 M of H_2O_2 were added under shaking at the desired temperature. The supernatant was separated using a magnet at certain time intervals to determine the dye consumption according to Eq. (2).

$$\frac{1}{[A]_t} - \frac{1}{[A]_0} = \mathrm{kt}, \tag{1}$$

$$\text{Dye consumption } (\%) = \frac{A_0 - A_t}{A_0} \times 100, \tag{2}$$

where A_0 is the dye absorbance at time 0, and A_t is the dye absorbance at time t (min).

Partial purification of HRP

Egyptian HRP was partially purified as follows (Mohamed et al. 2008). The HRP enzyme was extracted from horseradish roots (1 kg), cut into a cube, and juiced using a blender for 10 min. The extract was filtered through a Whatman filter paper and centrifuged at 8000 rpm and 25°C for 30 min. After centrifugation, the supernatant was identified as the crude extract, which was purified by ammonium sulfate precipitation (75% saturation). After centrifugation at 12,000×g for 20 min, the

precipitate was collected, dissolved in 50 mL of distilled water, and dialyzed against successive changes of distilled water. The dialysate was centrifuged using a nonbound protein filter (porous size: 0.45 μM, Millipore) at 15,000×*g* for 20 min to remove cell debris. The filtrate was lyophilized using a Christ Alpha 1-5 lyophilizer overnight to obtain HRP in powder form (Mohamed et al. 2008).

Determination of peroxidase activity

The peroxidase activity was examined spectrophotometrically through oxidation of guaiacol (2-methoxyphenyl) to tetraguaiacol at 470 nm (Tonami et al. 2004). The reaction mixture contained 1 mL of a 50 mM acetate buffer (pH 5.5), 40 mM guaiacol, 8 mM H_2O_2, and enzyme. The absorption at 470 nm changed considerably at room temperature because of guaiacol oxidation. The reaction mixture without the enzyme was used as a control. Enzyme activity is indicated as a unit; the amount of enzyme that can catalyze the oxidation of 1 μmol of guaiacol per minute at 30°C is defined as one unit of peroxidase activity.

Protein determination

The protein concentration in purified HRP was assessed using bovine serum albumin as a standard according to the Bradford method (He 2011). The protein concentration in immobilized HRP was estimated by eliminating the concentration of protein calculated in the supernatant before immobilization.

Enzyme characterization

The peroxidase activity of the free and immobilized enzyme was evaluated by determining the Michaelis constant (K_m) from the Lineweaver–Burk reciprocal plots (Lineweaver and Burk 1934). The values from the slopes and intercepts of the curves were calculated for different H_2O_2 and guaiacol concentrations ranging between 1.5 and 8 mM and between 8 and 40 mM, respectively, in an acetate buffer (pH 5.6). The effect of pH on the immobilized enzyme activity was analyzed in various buffer types, including a 50 mM sodium citrate buffer (pH 3.0–4.0), sodium acetate buffer (pH 5.0–5.6), sodium phosphate buffer (pH 6.0–8.0), and Tris-HCl buffer (pH 9) at 40°C. The effect of temperature was analyzed from 10 to 70°C, and the optimal temperature for the maximum activity of soluble and immobilized HRP was determined. The thermal stability of free and immobilized HRP was measured at different temperatures between 30 and 80°C after 30 min of incubation. The time intervals for the free and immobilized enzymes were also evaluated at the optimum temperature of 30°C, and the reusability of immobilized HRP was evaluated.

Results and discussion

Characterization of the biocatalyst

FT-IR analysis

The FT-IR spectra of Fe_3O_4, Fe_3O_4@NH_2, and Fe_3O_4@NH_2-HRP displayed in Fig. 1 show strong absorption bands around 420–600 and 3465 cm^{-1} attributable to Fe–O vibration and Fe–OH stretching, respectively. The grafting of APTES onto the magnetite surface was confirmed by the appearance of bands at 1430 and 2970 cm^{-1} corresponding to the bending and stretching vibrations of the –CH_2 group, respectively, in the spectrum of Fe_3O_4@NH_2. Besides, the band at 1048 cm^{-1} can be assigned to the symmetric stretching of the C–O bond. The band of the N–H stretching vibration of the terminal NH_2 group of APTES, which would be expected at 3300 cm^{-1}, was not observed because of its weak dipole moment (Araghi and Entezari 2015). The FT-IR spectrum of Fe_3O_4@NH_2-HRP displays the same characteristic bands as that of Fe_3O_4@NH_2. In addition, two new bands around 1640 cm^{-1} assigned to the presence of water/moisture, which prove the successful immobilization of HRP onto the Fe_3O_4@NH_2 surface.

XRD patterns

The XRD patterns of Fe_3O_4, Fe_3O_4@NH_2, and Fe_3O_4@NH_2-HRP are presented in Fig. 2. For all three samples, six characteristic peaks appeared at 2θ = 18°, 30.5°, 35.5°, 43°, 57°, and 63°, which can be assigned to the (111), (220), (311), (400), (511), and (440) planes, respectively. These results agree with those in the database (JCPDS-19-0629) for magnetite and confirm that the as-prepared magnetite exhibits a

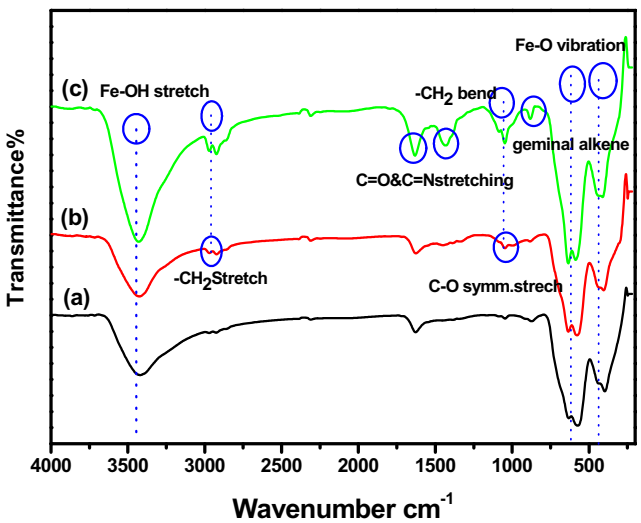

Fig. 1 The Fourier transform infrared spectra of **a** Fe_3O_4, **b** Fe_3O_4@NH_2, and **c** Fe_3O_4@NH_2-HRP

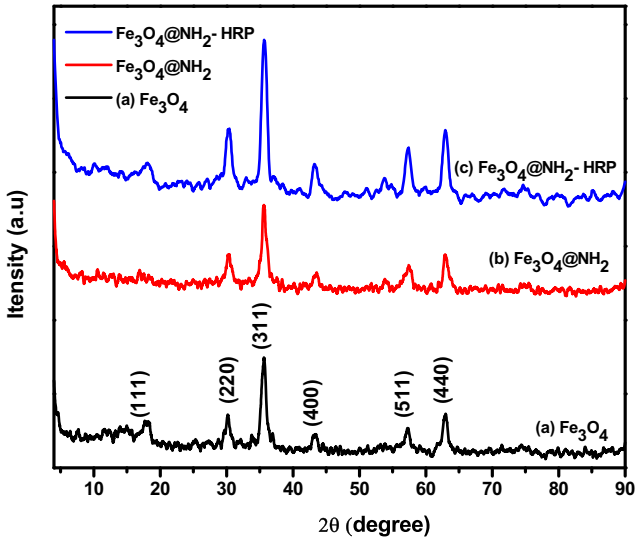

Fig. 2 X-ray diffraction patterns of **a** Fe_3O_4, **b** Fe_3O_4@NH_2, and **c** Fe_3O_4@NH_2-HRP

spinal cubic structure. Moreover, the crystalline structure of Fe_3O_4 NPs did not change after surface functionalization by APTES and HRP immobilization because both materials have an amorphous structure (Phan and Jones 2006). Changing the structure of enzyme protein is unexpected because the forces responsible for immobilization of enzyme are van der Waal and hydrogen bonds.

Vibrating sample magnetometry (VSM) study

The magnetization performance of Fe_3O_4, Fe_3O_4@NH_2, and Fe_3O_4@NH_2-HRP, with zero remanences and coercivity, confirmed the superparamagnetic behavior of the prepared samples (Mutneja et al. 2016). The magnetization saturation (Ms) values of Fe_3O_4, Fe_3O_4@NH_2, and Fe_3O_4@NH_2-HRP were determined to be 60.7, 59.1, and 63.6 emu/g, respectively (Fig. 3). The coating of pristine magnetite by a nonmagnetic

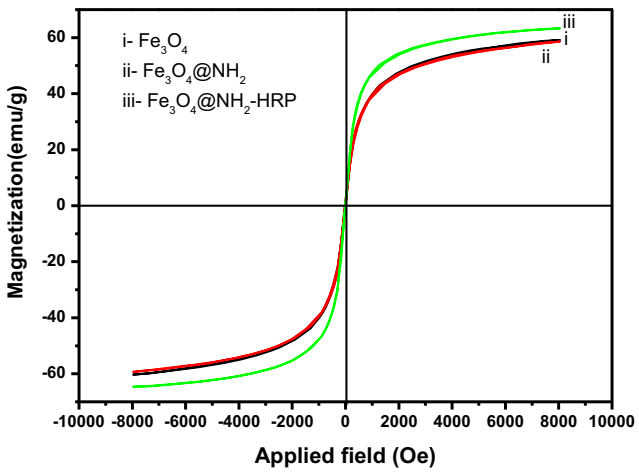

Fig. 3 Vibrating sample magnetometry hysteresis loops of (i) Fe_3O_4, (ii) Fe_3O_4@NH_2, and (iii) Fe_3O_4@NH_2-HRP

substance such as APTES is known to decrease the Ms value, whereas immobilization of HRP, which contains Fe ion in its chemical structure, increases the Ms value compared with that of pristine magnetite (Petcharoen and Sirivat 2012). Therefore, these results confirm the successful functionalization and immobilization steps. In any case, this does not result in the samples losing their separation ability under the influence of magnets.

TGA measurements

The functionalization with APTES and immobilization of HRP onto the Fe_3O_4 surface were confirmed using TGA curves illustrated in Fig. 4. For all three samples, the phase transition from magnetite (Fe_3O_4) to hematite (FeO) was observed above 570°C (Mahdavi et al. 2013). The TGA curves of both Fe_3O_4@NH_2 and Fe_3O_4@NH_2-HRP displayed a weight loss of 7.1% in a temperature range of 100–350°C, possibly due to the breakdown of grafted APTES molecules on the Fe_3O_4 surface. In addition, the TGA curve of Fe_3O_4@NH_2-HRP indicated a large weight loss of approximately 15% below 100°C, ascribable to physically adsorbed water onto the surface and immobilized HRP onto amine-functionalized Fe_3O_4 (Araghi and Entezari 2015).

BET, BJH, and zeta potential measurements

The BET specific surface area (S_{BET}) of Fe_3O_4 and Fe_3O_4@NH_2-HRP was determined to be 102.7 and 86.66 m^2/g, respectively, using the N_2 adsorption–desorption method (Venkateswarlu et al. 2013). This decrease in the S_{BET} value upon HRP immobilization can be ascribed to the occupation of the sites of the Fe_3O_4 surface by HRP (Sahoo et al. 2019). The isotherms of the two samples displayed hysteresis loops corresponding to type IV isotherms according to the IUPAC classification and occurred at relative pressures between 0.70 and 1.0, which confirms the presence of a

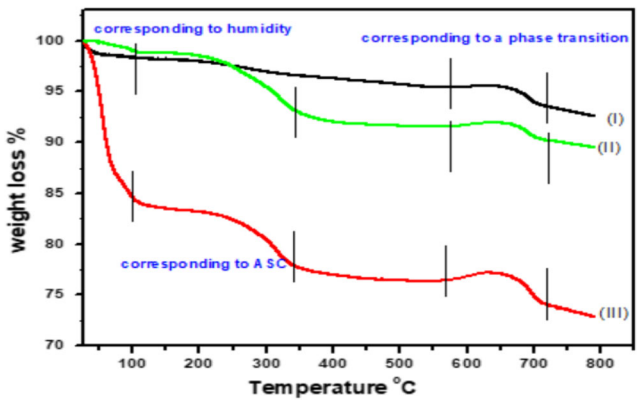

Fig. 4 Thermogravimetric analysis curves of (I) Fe_3O_4, (II) Fe_3O_4@NH_2, and (III) Fe_3O_4@NH_2-HRP

Table 1 Barrett–Joyner–Halenda data for estimating the porous nature of Fe_3O_4 and Fe_3O_4@NH_2-HRP

Sample	Surface area m^2/g	Pore volume cc/g	Pore radius nm	APR* nm	TPV* cc/g
Fe_3O_4	47.64	0.16	1.93	3.82×10^3	1.97×10^{-3}
Fe_3O_4@NH_2-HRP	46.11	0.14	1.93	3.85×10^3	1.67×10^{-3}

**APR*, average pore radius; *TPV*, total pore volume

mesoporous structure (Donohue and Aranovich 1999). Additionally, the porous nature and size distribution was determined by analyzing the desorption isotherm according to the BJH method, and the results are summarized in Table 1. Further information about the Fe_3O_4@NH_2-HRP catalyst surface was achieved by measuring the zeta potential; the resulting positive value (ζ = 23.23 mV) confirmed the rapid coagulation of dispersed Fe_3O_4@NH_2-HRP in solution (Ladole et al. 2014).

SEM and TEM studies

The textural morphologies of Fe_3O_4, Fe_3O_4@NH_2, and Fe_3O_4@NH_2-HRP are displayed in the SEM images depicted in (Fig. 5a–c), respectively. The images revealed a quasispherical structure with particle sizes below 70 nm. The Fe_3O_4 surface became smoother after functionalization by APTES, and a slight particle agglomeration was observed as a result of HRP addition (Ladole et al. 2014; Namdeo 2017). Further information was obtained from the TEM images presented in Fig. 5d–f (Enache et al. 2017), which revealed an agglomerated nanospherical morphology with an average grain size of 5–10 nm that did not increase after the immobilization step (Prasad et al. 2017). The crystalline nature of Fe_3O_4 was confirmed by the HRTEM image (Ma et al. 2003; Tang et al. 2011).

Kinetic measurements

The specific activity of free and immobilized HRP

The data indicated that HRP retained 72% of its activity after immobilization. In addition, the specific activity of immobilized HRP increased 1.2 times (from 3400 to 4149 U/mg) compared with that of free HRP, Table 2. These results stem from the fact that the free extract may contain many proteins including peroxidase, whereas not all proteins, apart from peroxidase, were immobilized on the matrix. This indicates that the immobilization step also serves for enzyme purification.

Michaelis constant (K_m) value and maximum velocity (V_{max}) of HRP

The process of immobilization affects the distribution of the substrate on the active sites of the enzyme (Mielgo et al. 2003). In the present study, the K_m values of free and immobilized HRP were determined to be 4.5 and 5 mM for H_2O_2 and 12.5 and 10 mM for guaiacol, respectively. Moreover, the V_{max} values of free and immobilized HRP were

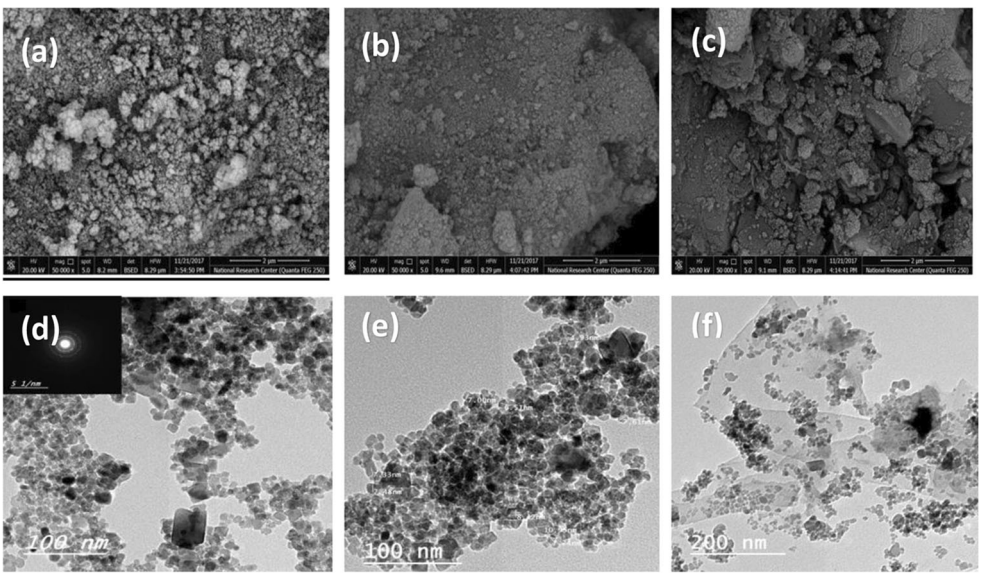

Fig. 5 Scanning electron microscopy images of **a** Fe_3O_4, **b** Fe_3O_4@NH_2, and **c** Fe_3O_4@NH_2-HRP and transmission electron microscopy images of **d** Fe_3O_4, **e** Fe_3O_4@NH_2, and **f** Fe_3O_4@NH_2-HRP

Table 2 Retention and specific activities of free and immobilized horseradish peroxidase (HRP) per gram

Step	Protein conc. mg	Enzyme activity U	Specific activity U/mg	Retention activity %
Free HRP	3.3	11,000	3400	-
Immobilized HRP	1.47	7920	4149	72

2.4 and 2 U for H_2O_2, respectively, and 1.25 U for guaiacol (Fig. 6a, b), which indicate the greater substrate affinity of immobilized HRP compared with the free enzyme. This improvement of the substrate affinity of the enzyme after functionalization may be attributed to the higher enzyme purity after immobilization mentioned above.

Effect of temperature and pH on the activity of free and immobilized HRP

As illustrated in Fig. 7a, the optimal temperature for the activity of free and immobilized HRP was approximately 40°C. Immobilized HRP exhibited a certain increase in the denaturation resistance with temperature. Thus, higher levels of catalytic activity were observed for the immobilized enzyme at temperatures above 40°C compared with the free enzyme (Kulshrestha and Husain 2006) because of the resistance of the immobilized enzyme to heat-induced conformational changes (Jun et al. 2019).

The pH value is related to the essential ionization status of the significant proton groups in the catalyst site of the enzyme. The pH–activity profile of free and immobilized HRP illustrated in Fig. 7b revealed that the optimal pH was 5.6 in both cases. This agrees with the results reported for most plant peroxidases, which exhibit optimum activity between 4.5 and 6.0 (Diao et al. 2014). Moreover, Jun et al. reported that immobilized HRP exhibited higher enzymatic activity at a broader pH range compared with the free enzyme (Jun et al. 2019). The strong covalent attachment of the enzyme molecules to the support matrix increases the pH stability of immobilized HRP according to Eq. (3). Immobilized enzymes are particularly resistant to environmental changes due to strong intermolecular interactions (Jun et al. 2019). Furthermore, stable binding with the support material prevents conformational changes of enzymes under extreme pH conditions, thereby restricting their denaturation (Ahmad and Khare 2018). Immobilized enzymes are more tolerant to acidic and alkaline environments; this renders them suitable for a variety of applications (Sun et al. 2017).

$$\text{Relative activity } (\%) = \frac{\text{Enzyme activity at the specific pH (or temperature)}}{\text{Enzyme activity at the optimum pH (or temperature)}} \times 100 \quad (3)$$

Impact of temperature on HRP stability

To assess the thermal stability of free and immobilized HRP, both enzymes were exposed to different temperatures (30–80°C) and incubated for 30 min. As can be observed in Fig. 8, the maximum activity was retained up to 40°C for free HRP and 50°C for immobilized HRP. Upon increasing the temperature further, the activity of free HRP was completely inhibited after 30 min at 70°C, whereas immobilized HRP retained 25% of its original activity. Thus, immobilization increased significantly the thermostability. Similar results were previously reported for immobilized HRP on APTMS, which maintained its full activity at 60°C for at least 2 h, whereas the activity of free HRP decreased to nearly zero at the same temperature (Tupper et al. 2010). Likewise, immobilized turnip peroxidase incubated at 60°C for 2 h retained 54% of the initial enzyme activity, whereas the soluble enzyme lost almost 83% of the original activity under

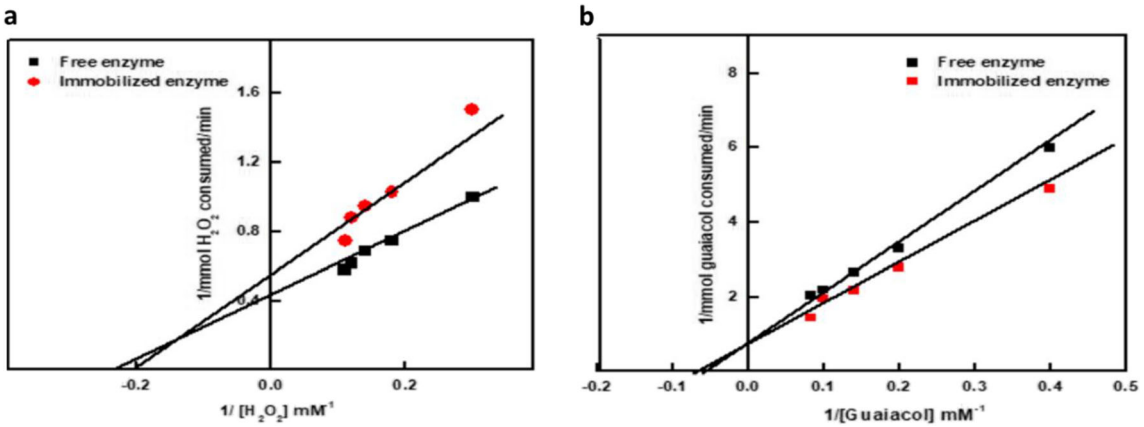

Fig. 6 Lineweaver–Burk plots for the reaction velocity of free HRP and immobilized HRP to **a** H_2O_2 and **b** guaiacol concentrations

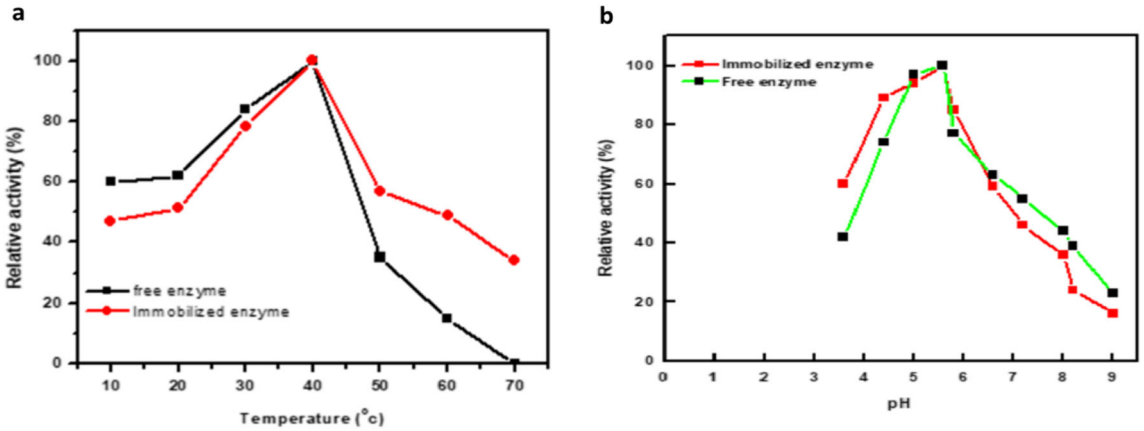

Fig. 7 **a** Effect of temperature on the activity of free and immobilized HRP at various temperatures. **b** Effect of pH on the activity of free and immobilized HRP

similar incubation conditions (Xu and Wang 2010). The relative activity (%) was calculated from the ratio of the activity after incubation to the activity at the optimum temperature of incubation.

Thermal stability of free and immobilized HRP

The thermal stability trends of the free and immobilized enzyme in terms of relative activity at 30°C are compared in Fig. 9. Immobilized HRP retained its relative activity after 4 h, whereas the free enzyme lost a significant amount of activity under similar operating conditions. Furthermore, previous research has demonstrated that immobilization improves the thermal stability of enzymes (Li et al. 2017). The thermal stability of mounted enzymes was increased by the strong noncovalent interaction between enzyme molecules and the Fe_3O_4 surface support (Sun et al. 2017). At high temperatures, the strong noncovalent bonding prevents protein mobility, adding rigidity to the enzyme structure and preventing denaturation. As a result, these findings revealed that immobilization had a considerable impact on the thermal stability of the enzyme (Sun et al. 2017).

Reusability

Generally, the use of an immobilized biocatalyst offers increased stability and easy separation of the bound peroxidase during washes (Mohamed et al. 2014). To evaluate the reusability of immobilized HRP, Fig. 10, a single reaction cycle was performed in 1.0 mL of the reaction mixture containing 0.1 unit of immobilized HRP, 8 mM H_2O_2, 40 mM guaiacol, and a 50 mM sodium acetate buffer (pH 5.6). Then, immobilized HRP was washed with a sodium acetate buffer (pH 5.6) to remove any residual substrate and added to the following reaction cycle. In each reaction cycle, the percentage of relative activity was calculated as the ratio of the enzyme activity to the ratio of the enzyme activity of the first reaction cycle.

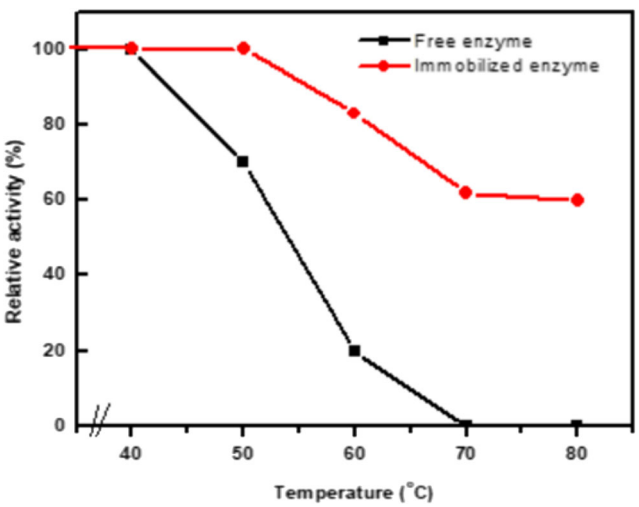

Fig. 8 Effect of temperature on the activity of free and immobilized HRP

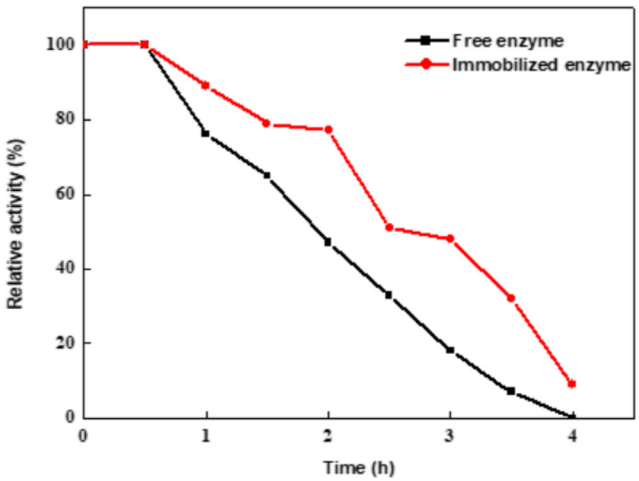

Fig. 9 Thermal stability of immobilized and free horseradish peroxidase at the optimum temperature of 30°C

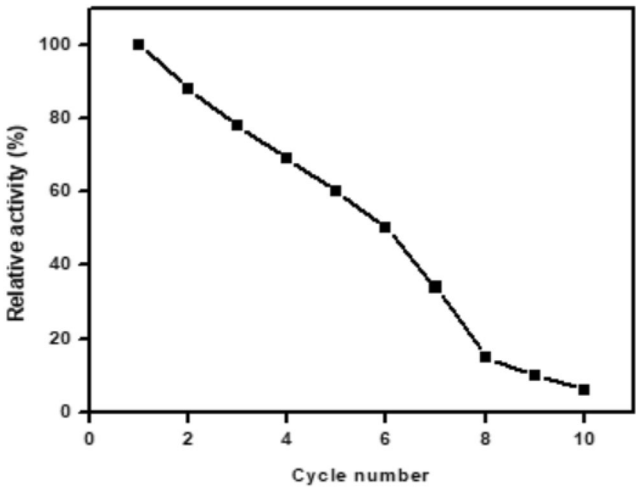

Fig. 10 Reusability of immobilized HRP on Fe_3O_4@NH_2 by washing repeatedly following each test, using 1.0 mL of a reaction mixture containing 8 mM H_2O_2, 40 mM guaiacol, and 50 mM sodium acetate buffer (pH 5.6)

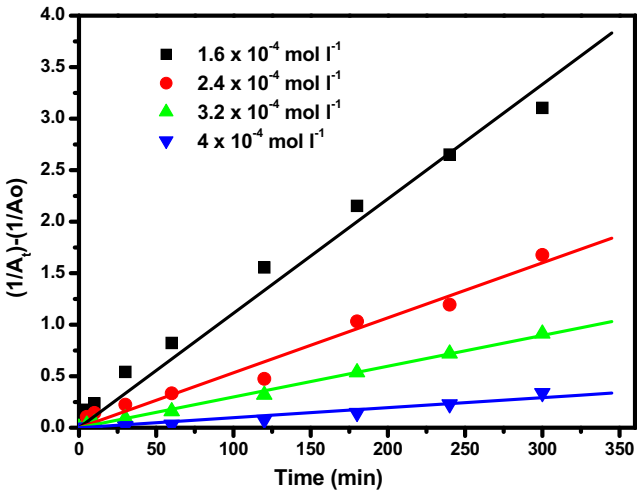

Fig. 12 Second-order plots for the oxidative degradation of the acid black-HC dye. [Fe_3O_4@NH_2-HRP] = 300 mg L^{-1}, $[H_2O_2]_o$ = 0.16 mol L^{-1}, and pH = 5.6 at 37°C

Kinetics of the oxidative degradation of the AB dye

Effect of pH

The oxidation rate of the AB dye with H_2O_2 catalyzed by Fe_3O_4@NH_2-HRP was determined at different pH values. The pH of the AB dye solution was set to 5.6 with an acetate buffer, 9.6 with a carbonate–bicarbonate buffer, and 2.6 with a glycine–HCl buffer. As illustrated in Fig. 11, the oxidation rate of the AB dye decreased with increasing pH value; this is in accord with the Fenton reaction mechanism (Pereira et al. 2012).

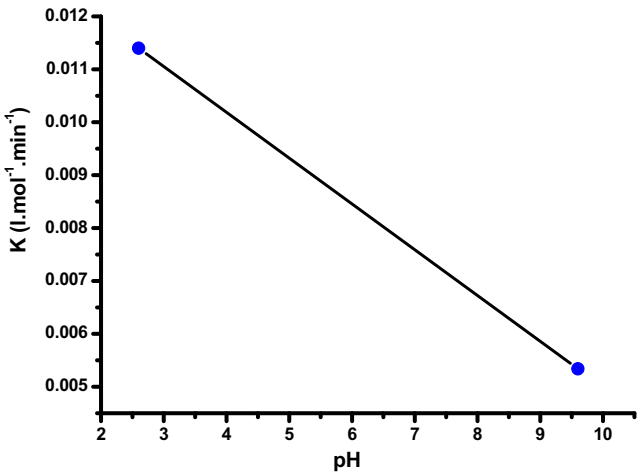

Fig. 11 pH dependence of the oxidation rate of the acid black-HC dye, $[AB]_o$ = 2.4 × 10^{-4} mol L^{-1}, [Fe_3O_4@NH_2-HRP] = 300 mg L^{-1}, and $[H_2O_2]_o$ = 0.16 mol L^{-1} at 37°C

Effect of the concentration of the AB dye

The dependency of the reaction rate on $[AB]_o$ was calculated by changing the concentration between 1.6 × 10^{-4} mol L^{-1} and 4 × 10^{-4} mol L^{-1} while keeping the concentration of other reaction constituents constant. The AB dye consumption in the presence of Fe_3O_4@NH_2-HRP as a function of time is described as second-order plots at 37 °C in Fig. 12. The values of the rate constants obtained from the second-order plots decreased with increasing AB from 1.6 × 10^{-4} mol L^{-1} to 4 × 10^{-4} mol L^{-1}. This behavior can be attributed to the restricted number of $HO^{\bullet}$ radicals involved in the oxidation process (Dulman et al. 2012).

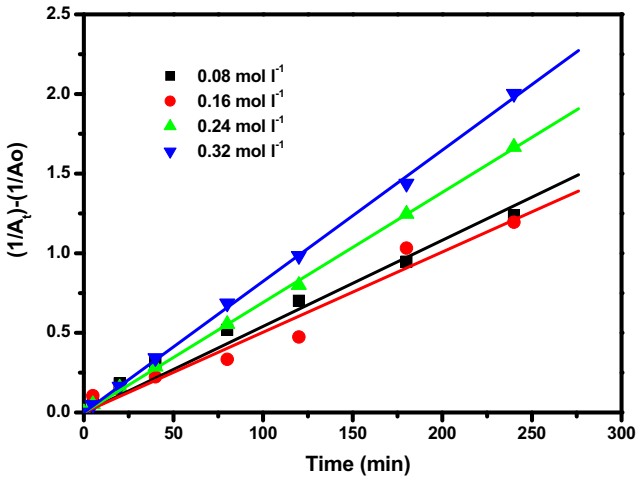

Fig. 13 Second-order plots for the degradation of the acid black-HC (AB) dye as a function of time at different H_2O_2 concentrations. [Fe_3O_4@NH_2-HRP] = 300 mg L^{-1}, $[AB]_o$ = 2.4 × 10^{-4} mol L^{-1}, and pH = 5.6 at 37°C

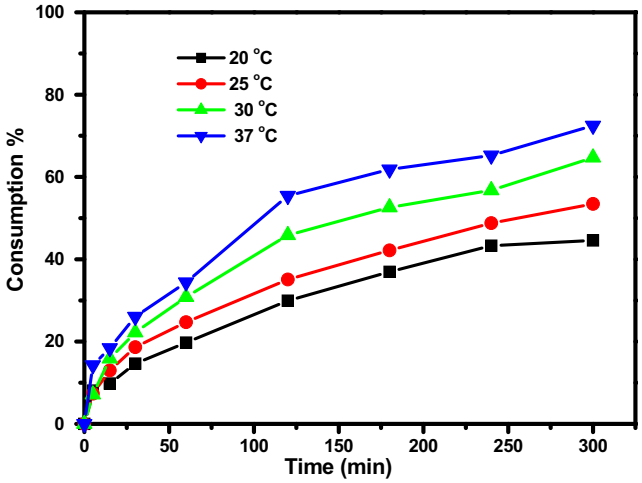

Fig. 14 Consumption of the acid black-HC dye as a function of time at different temperatures

Effect of the H_2O_2 concentration

The dependency of the oxidation rate of the AB dye on the H_2O_2 concentration was calculated by changing the H_2O_2 concentration between 0.08 and 0.32 mol L^{-1}. The second-order plots for the oxidative degradation reaction of AB are shown in Fig. 13. The oxidation rate slightly decreased and then increased $[H_2O_2]_o$, while keeping the concentration of other reactants constant. A plausible explanation for this phenomenon is that immobilized HRP consumed a high amount of H_2O_2 to reach its maximum activity to produce $HO^{\bullet}$ for AB dye degradation (Zhu et al. 2011).

Effect of temperature

The effect of temperature on the AB dye decolorization was investigated over a temperature range of 20–37°C. The concentrations of AB, H_2O_2, and Fe_3O_4@NH_2-HRP were set to 0.16 mol L^{-1}, 2.4 × 10^{-4} mol L^{-1}, and 300 mg L^{-1}, respectively. Fig. 14 indicates that the consumption of AB increased as a function of time with increasing temperature, thus confirming that the oxidation of AB using the Fe_3O_4@NH_2-HRP catalyst is an endothermic process.

Table 3 Thermodynamic parameters of the oxidative consumption of the acid black-HC dye

Catalyst	Temp °C	$k \times 10^{-3}$ L mol^{-1} min^{-1}	E_a k J mol^{-1}	$\Delta H^{\#}$ k J mol^{-1}	$\Delta G^{\#}$ k J mol^{-1}	$\Delta S^{\#}$ J mol^{-1} K^{-1}
Fe_3O_4@NH_2-HRP	20	1.93	47.86	45.41	42.92	−142.44
	25	2.55				
	30	3.85				
	37	5.53				

The thermodynamic activation parameters, $\Delta S^{\#}$, and $\Delta H^{\#}$ were determined from the intercept and the slope of the plots, respectively, according to Eq. (4) and the Eyring plot depicted in Fig. 15. Besides, the activation energy (E_a) and free energy ($\Delta G^{\#}$) were estimated from Eqs. (5) and (6), respectively, and the results are summarized in Table 3. The negative sign of the entropy value indicates that the reaction is endothermic.

$$\ln\left(\frac{k}{T}\right) = -\frac{\Delta H^{\#}}{\mathrm{RT}} + \ln\left(\frac{k_B}{h}\right)\frac{\Delta S^{\#}}{R}, \tag{4}$$

$$E_a = \Delta H^{\#} + \mathrm{RT}_{\mathrm{exp}}, \tag{5}$$

$$\Delta G^{\#} = \Delta H^{\#} - T_{\mathrm{exp}}\Delta S^{\#}, \tag{6}$$

where, h, k_B, and R are Planck's, Boltzmann, and ideal gas constants, respectively, and T_{exp} is the average experimental temperature.

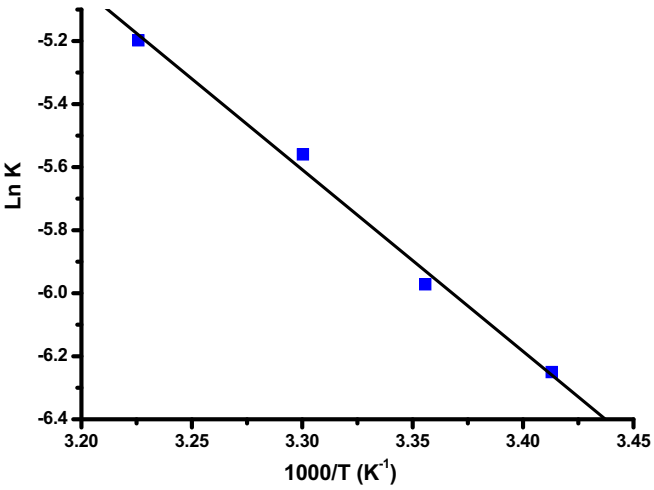

Fig. 15 Eyring plot for the oxidative degradation of the acid black-HC dye with $[H_2O_2]_o$ = 0.16 mol L^{-1} and [Fe_3O_4@NH_2-HRP] = 300 mg L^{-1}

Conclusion

In summary, Fe_3O_4 was prepared using the coprecipitation method and subsequently functionalized with APTES. Then, immobilization of HRP on the $Fe_3O_4@NH_2$ surface provided favorable operational, thermal, and storage stability compared with that of free HRP. In addition, we use the simplest physical adsorption in the immobilization protocol to decrease immobilization cost and using paramagnetic non-porous materials to avoid decreasing in non-flexible and handle in the reactor that increases from an enzyme loading and the volumetric activity that has an impact on AB degradation efficiency. The oxidation of the AB dye using immobilized HRP as a biocatalyst is an endothermic process. The AB dye degradation involves an initial cleavage of the azo (*N*=*N*) linkage followed by oxidative cleavage of the C–S bond of the dye by free radicals generated in the intermediate, producing carbon dioxide and water. The results of this study demonstrate the applicability of $Fe_3O_4@NH_2$-HRP as an effective biocatalyst for the degradation of an azo dye in an aqueous solution.

Supplementary Information The online version contains supplementary material available at https://doi.org/10.1007/s11356-021-16119-z.

Author contribution BK: Methodology, Writing—Original draft preparation. AG: Conceptualization, Supervision, Investigation. AK: Formal analysis, Reviewing, and Editing.

Funding This research project is funded by the Research Fund—Tanta University (TU- 03-16).

Data availability Please contact the authors for data requests.

Declarations

Ethical approval and consent to participate Not applicable.

Consent for publication Not applicable.

Competing interests The authors declare no competing interests.

References

Ahmad R, Khare SK (2018) Immobilization of Aspergillus niger cellulase on multiwall carbon nanotubes for cellulose hydrolysis. Bioresour Technol 252:72–75. https://doi.org/10.1016/j.biortech.2017.12.082

Ali M, Husain Q, Sultana S, Ahmad M (2018) Immobilization of peroxidase on polypyrrole-cellulose-graphene oxide nanocomposite via non-covalent interactions for the degradation of Reactive Blue 4 dye. Chemosphere 202:198–207. https://doi.org/10.1016/j.chemosphere.2018.03.073

Araghi SH, Entezari MH (2015) Amino-functionalized silica magnetite nanoparticles for the simultaneous removal of pollutants from aqueous solution. Appl Surf Sci 333:68–77. https://doi.org/10.1016/j.apsusc.2015.01.211

Bilal M, Iqbal HMN (2021) Armoring bio-catalysis via structural and functional coordination between nanostructured materials and lipases for tailored applications. Int J Biol Macromol 166:818–838. https://doi.org/10.1016/j.ijbiomac.2020.10.239

Bilal M, Iqbal HM, Shah SZH, Hu H, Wang W, Zhang X (2016) Horseradish peroxidase-assisted approach to decolorize and detoxify dye pollutants in a packed bed bioreactor. J Environ Manag 183:836–842. https://doi.org/10.1016/j.jenvman.2016.09.040

Bilal M, Asgher M, Parra-Saldivar R, Hu H, Wang W, Zhang X, Iqbal HM (2017a) Immobilized ligninolytic enzymes: an innovative and environmental responsive technology to tackle dye-based industrial pollutants–a review. Sci Total Environ 576:646–659. https://doi.org/10.1016/j.scitotenv.2016.10.137

Bilal M, Iqbal HM, Hu H, Wang W, Zhang X (2017b) Enhanced biocatalytic performance and dye degradation potential of chitosan-encapsulated horseradish peroxidase in a packed bed reactor system. Sci Total Environ 575:1352–1360. https://doi.org/10.1016/j.scitotenv.2016.09.215

Boudrant J, Woodley JM, Fernandez-Lafuente R (2020) Parameters necessary to define an immobilized enzyme preparation. Process Biochem 90:66–80. https://doi.org/10.1016/j.procbio.2019.11.026

Cipolatti EP, Valerio A, Henriques RO, Moritz DE, Ninow JL, Freire DM, Manoel EA, Fernandez-Lafuente R, de Oliveira D (2016) Nanomaterials for biocatalyst immobilization–state of the art and future trends. RSC Adv 6(106):104675–104692. https://doi.org/10.1039/c6ra22047a

Diao M, Ayékoué BN, Dibala D, Dabonné S, Dicko MH (2014) Purification and characterization of sweet potato (Ipomoea Batatas) peroxidase. J Anim Plant Sci 22:3419–3432

Ding S, Cargill AA, Medintz IL, Claussen JC (2015) Increasing the activity of immobilized enzymes with nanoparticle conjugation. Curr Opin Biotechnol 34:242–250. https://doi.org/10.1016/j.copbio.2015.04.005

Donadelli JA, Einschlag FSG, Laurenti E, Magnacca G, Carlos L (2018) Soybean peroxidase immobilized onto silica-coated superparamagnetic iron oxide nanoparticles: effect of silica layer on the enzymatic activity. Colloids Surf B: Biointerfaces 161:654–661. https://doi.org/10.1016/j.colsurfb.2017.11.043

Donohue MD, Aranovich G (1999) A new classification of isotherms for Gibbs adsorption of gases on solids. Fluid Phase Equilib 158:557–563. https://doi.org/10.1016/S0378-3812(99)00074-6

Dulman V, Cucu-Man SM, Olariu RI, Buhaceanu R, Dumitraş M, Bunia I (2012) A new heterogeneous catalytic system for decolorization and mineralization of Orange G acid dye based on hydrogen peroxide and a macroporous chelating polymer. Dyes Pigments 95:79–88. https://doi.org/10.1016/j.dyepig.2012.03.024

El-Alaily T, El-Nimr M, Saafan S, Kamel M, Meaz T, Assar S (2015) Construction and calibration of a low cost and fully automated vibrating sample magnetometer. J Magn Magn Mater 386:25–30. https://doi.org/10.1016/j.jmmm.2015.03.051

Enache DF, Vasile E, Simonescu CM, Răzvan A, Nicolescu A, Nechifor AC, Oprea O, Pătescu RE, Onose C, Dumitru F (2017) Cysteine-functionalized silica-coated magnetite nanoparticles as potential nanoadsorbents. J Solid State Chem 253:318–328. https://doi.org/10.1016/j.jssc.2017.06.013

Garcia-Galan C, Berenguer-Murcia Á, Fernandez-Lafuente R, Rodrigues RC (2011) Potential of different enzyme immobilization strategies to improve enzyme performance. Adv Synth Catal 353(16):2885–2904. https://doi.org/10.1002/adsc.201100534

Gemeay AH, Keshta BE, El-Sharkawy RG, Zaki AB (2019) Chemical insight into the adsorption of reactive wool dyes onto amine-functionalized magnetite/silica core-shell from industrial wastewaters. Environ Sci Pollut Res Int 27:32341–32358. https://doi.org/10.1007/s11356-019-06530-y

Guzik U, Hupert-Kocurek K, Wojcieszyńska D (2014) Immobilization as a strategy for improving enzyme properties-application to

oxidoreductases. Molecules 19:8995–9018. https://doi.org/10.3390/molecules19078995

He F (2011) Bradford protein assay. Bio 101:e45. https://doi.org/10.21769/BioProtoc.45

Hoffmann C, Grundtvig IP, Thrane J, Garg N, Gernaey KV, Pinelo M, Woodley JM, Krühne U, Daugaard AE (2018) Experimental and computational evaluation of area selectively immobilized horseradish peroxidase in a microfluidic device. Chem Eng J 332:16–23. https://doi.org/10.1016/j.cej.2017.09.050

Hosseinifar A, Shariaty-Niassar M, Seyyed Ebrahimi S, Moshref-Javadi M (2017) Synthesis, characterization, and application of partially blocked amine-functionalized magnetic nanoparticles. Langmuir 33:14728–14737. https://doi.org/10.1021/acs.langmuir.7b02093

Iyer PV, Ananthanarayan L (2008) Enzyme stability and stabilization—aqueous and non-aqueous environment. Process Biochem 43(10):1019–1032. https://doi.org/10.1016/j.procbio.2008.06.004

Jesionowski T, Zdarta J, Krajewska B (2014) Enzyme immobilization by adsorption: a review. Adsorption. 20(5-6):801–821. https://doi.org/10.1007/s10450-014-9623-y

Jun LY, Mubarak NM, Yon LS, Bing CH, Khalid M, Jagadish P, Abdullah EC (2019) Immobilization of peroxidase on functionalized MWCNTs-buckypaper/polyvinyl alcohol nanocomposite membrane. Sci Rep 9(1):2215. https://doi.org/10.1038/s41598-019-39621-4

Katchalski-Katzir E (1993) Immobilized enzymes–learning from past successes and failures. Trends Biotechnol 11:471–478. https://doi.org/10.1016/0167-7799(93)90080-S

Kulshrestha Y, Husain Q (2006) Bioaffinity-based an inexpensive and high yield procedure for the immobilization of turnip (Brassica rapa) peroxidase. Biomol Eng 23:291–297. https://doi.org/10.1016/j.bioeng.2006.07.004

Kumar V, Misra N, Goel NK, Thakar R, Gupta J, Varshney L (2016) A horseradish peroxidase immobilized radiation grafted polymer matrix: a biocatalytic system for dye waste water treatment. RSC Adv 6:2974–2981. https://doi.org/10.1039/C5RA20513A

Ladole MR, Muley AB, Patil ID, Talib M, Parate VR (2014) Immobilization of tropizyme-P on amino-functionalized magnetic nanoparticles for fruit juice clarification. J Biochem Tech 5:838–845

Li ZL, Cheng L, Zhang LW, Liu W, Ma WQ, Liu L (2017) Preparation of a novel multi-walled-carbon-nanotube/cordierite composite support and its immobilization effect on horseradish peroxidase. Process Saf Environ Prot 107:463–467. https://doi.org/10.1016/j.psep.2017.02.021

Lineweaver H, Burk D (1934) The determination of enzyme dissociation constants. J Am Chem Soc 56:658–666. https://doi.org/10.1021/ja01318a036

Liu Y, Li Y, Li X-M, He T (2013) Kinetics of (3-aminopropyl) triethoxylsilane (APTES) silanization of superparamagnetic iron oxide nanoparticles. Langmuir 29:15275–15282. https://doi.org/10.1021/la403269u

López-Serrano P, Cao L, Van Rantwijk F, Sheldon RA (2002) Cross-linked enzyme aggregates with enhanced activity: application to lipases. Biotechnol Lett 24(16):1379–1383

Lyddiatt A (2002) Process chromatography: current constraints and future options for the adsorptive recovery of bioproducts. Curr Opin Biotechnol 13(2):95–103. https://doi.org/10.1016/s0958-1669(02)00293-8

Ma M, Zhang Y, Yu W, Shen H-y, Zhang H-q GN (2003) Preparation and characterization of magnetite nanoparticles coated by amino silane. Colloids Surf A Physicochem Eng Asp 212:219–226. https://doi.org/10.1016/S0927-7757(02)00305-9

Mahdavi M, Ahmad MB, Haron MJ, Namvar F, Nadi B, Rahman MZA, Amin J (2013) Synthesis, surface modification and characterisation of biocompatible magnetic iron oxide nanoparticles for biomedical applications. Molecules 18:7533–7548. https://doi.org/10.3390/molecules18077533

Mateo C, Palomo JM, Fernandez-Lorente G, Guisan JM, Fernandez-Lafuente R (2007) Improvement of enzyme activity, stability and selectivity via immobilization techniques. Enzyme Microb. Technol. 40(6):1451–1463. https://doi.org/10.1016/j.enzmictec.2007.01.018

Mielgo I, Palma C, Guisan J, Fernandez-Lafuente R, Moreira M, Feijoo G, Lema J (2003) Covalent immobilisation of manganese peroxidases (MnP) from Phanerochaete chrysosporium and Bjerkandera sp. BOS55. Enzyme Microb. Technol. 32:769–775. https://doi.org/10.1016/S0141-0229(03)00066-8

Min K, Yoo YJ (2014) Recent progress in nanobiocatalysis for enzyme immobilization and its application. Biotechnol Bioprocess Eng 19:553–567. https://doi.org/10.1007/s12257-014-0173-7

Mohamed SA, Aly A, Mohamed TM, Salah HA (2008) Immobilization of horseradish peroxidase on nonwoven polyester fabric coated with chitosan. Appl Biochem Biotechnol 144:169–179. https://doi.org/10.1007/s12010-007-8026-x

Mohamed TM, El-Souod SMA, Ali EM, El-Badry MO, El-Keiy MM, Aly AS (2014) Immobilization and characterization of inulinase from Ulocladium atrum on nonwoven fabrics. J Biosci 39:785–793. https://doi.org/10.1007/s12038-014-9477-1

Mutneja R, Singh R, Kaur V, Wagler J, Fels S, Kroke E (2016) Schiff base tailed silatranes for the fabrication of functionalized silica based magnetic nano-cores possessing active sites for the adsorption of copper ions. New J Chem 40:1640–1648. https://doi.org/10.1039/C5NJ02287H

Namdeo M (2017) Magnetite nanoparticles as effective adsorbent for water purification: a review. Adv Recycling Waste Manag 2:126–129. https://doi.org/10.4172/2475-7675.1000135

Nanayakkara S, Zhao Z, Patti AF, He L, Saito K (2014) Immobilized horseradish peroxidase (I-HRP) as biocatalyst for oxidative polymerization of 2, 6-dimethylphenol. ACS Sustain Chem Eng 2:1947–1950. https://doi.org/10.1021/sc500392k

Pandey VP, Awasthi M, Singh S, Tiwari S, Dwivedi UN (2017) A comprehensive review on function and application of plant peroxidases. Biochem Anal Biochem 6:308. https://doi.org/10.4172/2161-1009.1000308

Pasternack RM, Rivillon Amy S, Chabal YJ (2008) Attachment of 3-(aminopropyl) triethoxysilane on silicon oxide surfaces: dependence on solution temperature. Langmuir 24:12963–12971. https://doi.org/10.1021/la8024827

Pereira M, Oliveira L, Murad E (2012) Iron oxide catalysts: Fenton and Fentonlike reactions–a review. Clay Miner 47:285–302. https://doi.org/10.1180/claymin.2012.047.3.01

Petcharoen K, Sirivat A (2012) Synthesis and characterization of magnetite nanoparticles via the chemical co-precipitation method. Mater Sci Eng B 177:421–427. https://doi.org/10.1016/j.mseb.2012.01.003

Phan NT, Jones CW (2006) Highly accessible catalytic sites on recyclable organosilane-functionalized magnetic nanoparticles: an alternative to functionalized porous silica catalysts. J Mol Catal 253:123–131. https://doi.org/10.1016/j.molcata.2006.03.019

Prasad C, Yuvaraja G, Venkateswarlu P (2017) Biogenic synthesis of Fe3O4 magnetic nanoparticles using Pisum sativum peels extract and its effect on magnetic and Methyl orange dye degradation studies. J Magn Magn Mater 424:376–381. https://doi.org/10.1016/j.jmmm.2016.10.084

Ramalingam B, Parandhaman T, Choudhary P, Das SK (2018) Biomaterial functionalized graphene-magnetite nanocomposite: a novel approach for simultaneous removal of anionic dyes and heavy-metal ions. ACS Sustain Chem Eng 6:6328–6341. https://doi.org/10.1021/acssuschemeng.8b00139

Rudra S, Shivhare U, Basu S, Sarkar B (2008) Thermal inactivation kinetics of peroxidase in coriander leaves. Food Bioprocess Technol 1:187–195. https://doi.org/10.1007/s11947-007-0013-2

Sahoo JK, Paikra SK, Mishra M, Sahoo H (2019) Amine functionalized magnetic iron oxide nanoparticles: synthesis, antibacterial activity and rapid removal of Congo red dye. J Mol Liq 282:428–440. https://doi.org/10.1016/j.molliq.2019.03.033

Sun H, Jin X, Long N, Zhang R (2017) Improved biodegradation of synthetic azo dye by horseradish peroxidase cross-linked on nano-composite support. Int J Biol Macromol 95:1049–1055. https://doi.org/10.1016/j.ijbiomac.2016.10.093

Tang T, Fan H, Ai S, Han R, Qiu Y (2011) Hemoglobin (Hb) immobilized on amino-modified magnetic nanoparticles for the catalytic removal of bisphenol A. Chemosphere 83:255–264. https://doi.org/10.1016/j.chemosphere.2010.12.075

Tomotani EJ, Vitolo M (2006) Method for immobilizing invertase by adsorption on Dowex® anionic exchange resin. Braz J Pharm Sci 42:245–249. https://doi.org/10.1590/S1516-93322006000200009

Tonami H, Uyama H, Nagahata R, Kobayashi S (2004) Guaiacol oxidation products in the enzyme-activity assay reaction by horseradish peroxidase catalysis. Chem Lett 33:796–797. https://doi.org/10.1246/cl.2004.796

Tong XD, Dong XY, Sun Y (2002) Lysozyme adsorption and purification by expanded bed chromatography with a small-sized dense adsorbent. Biochem Eng J 12(2):117–124. https://doi.org/10.1016/S1369-703X(02)00063-3

Tupper J, Stratford M, Hill S, Tozer G, Dachs G (2010) In vivo characterization of horseradish peroxidase with indole-3-acetic acid and 5-bromoindole-3-acetic acid for gene therapy of cancer. Cancer Gene Ther 17:420–428. https://doi.org/10.1038/cgt.2009.86

Venkateswarlu S, Rao YS, Balaji T, Prathima B, Jyothi N (2013) Biogenic synthesis of Fe3O4 magnetic nanoparticles using plantain peel extract. Mater Lett 100:241–244. https://doi.org/10.1016/j.matlet.2013.03.018

Vineh MB, Saboury AA, Poostchi AA, Mamani L (2018a) Physical adsorption of horseradish peroxidase on reduced graphene oxide nanosheets functionalized by amine: a good system for biodegradation of high phenol concentration in wastewater. Int J Environ Res 12:45–57. https://doi.org/10.1007/s41742-018-0067-1

Vineh MB, Saboury AA, Poostchi AA, Rashidi AM, Parivar K (2018b) Stability and activity improvement of horseradish peroxidase by covalent immobilization on functionalized reduced graphene oxide and biodegradation of high phenol concentration. Int J Biol Macromol 106:1314–1322. https://doi.org/10.1016/j.ijbiomac.2017.08.133

Williams A, Frasca V (2001) Ion-exchange chromatography. Curr Protoc Protein Sci. Chapter 8:Unit8.2 15. https://doi.org/10.1002/0471140864.ps0802s15

Xu Q, Wang M (2010) Effect of electric field on horseradish peroxidase activity and its structure. In: 2010 3rd International Conference on Biomedical Engineering and Informatics. IEEE, New York, pp 1307–1309. https://doi.org/10.1109/BMEI.2010.5639251

Yang Y, Zhao M, Yao P, Huang Y, Dai Z, Yuan H, Ni C (2018) Comparative studies on enzyme activity of immobilized horseradish peroxidase in silica nanomaterials with three different shapes and methoxychlor degradation of vesicle-like mesoporous SiO2 as carrier. J Nanosci Nanotechnol 18:2971–2978. https://doi.org/10.1166/jnn.2018.14300

Zhang Y, Wu H, Huang X, Zhang J, Guo S (2011) Effect of substrate (ZnO) morphology on enzyme immobilization and its catalytic activity. Nanoscale Res Lett 6:1–7. https://doi.org/10.1186/1556-276X-6-450

Zhu H, Hu Y, Jiang G, Shen G (2011) Peroxidase-like activity of aminopropyltriethoxysilane-modified iron oxide magnetic nanoparticles and its application to clenbuterol detection. Eur Food Res Technol 233:881–887. https://doi.org/10.1007/s00217-011-1582-x